Experiments in Fluids 36 (2004) 783–790
DOI 10.1007/s00348-003-0760-4

The optimal drop shape for vortices generated by drop impacts: the effect of surfactants on the drop surface

J. R. Saylor, N. K. Grizzard

Abstract Subsurface vortices are frequently created when a falling drop strikes a flat water surface. Prior work has demonstrated that the shape of the drop at the point of impact is critical in determining how deep or how fast the resulting vortex will penetrate into the water bulk. In the present study, the details of this phenomena are explored by using surfactants to vary surface tension. Specifically, Triton X-100 monolayers are created on the surface of the drop, and on the flat water surface. The results of these experiments suggest that there is no single optimal drop shape resulting in best vortex penetration. Rather, the data suggest that the optimal shape depends on the surface tension of the falling drop. An attempt is made to reconcile contradictory results in the literature using this result.

1 Introduction

The impact of a falling water drop with a flat water surface can result in the formation of a vortex ring. These vortex rings are easily visualized by including a dye in the drop fluid. When this is done, the vortex appears as a toroidal mass, or ring, which propagates away from the impact site, into the bulk, taking most of the dyed fluid with it. A "stalk" of dyed fluid is also observed trailing behind the vortex, marking a line along the direction of travel. These vortex rings do not necessarily mark the location of vorticity, but rather the location of the drop fluid. Therefore, an investigation of vortices created using dyed drops (such as the one described herein) reveals the ultimate location of the drop fluid. This is significant since an application of the work presented here is the entrainment of oxygen into the water bulk during rain.

Received: 30 January 2003 / Accepted: 10 November 2003
Published online: 18 March 2004

J. R. Saylor (✉), N. K. Grizzard
Department of Mechanical Engineering,
Clemson University, Clemson, SC29634, USA
E-mail: jrsaylor@ces.clemson.edu
Tel.: +1-864-6565621
Fax: +1-864-6564435

The authors thank Professor Donald E. Beasley for loaning several crucial pieces of instrumentation. Financial support from the Clemson University Department of Mechanical Engineering is gratefully acknowledged.

Drop-induced vortex rings can travel a significant depth into the water bulk at velocities in excess of 100 mm/sec. The exact mechanism by which these vortices are formed is unclear, although several ideas have been put forth to explain vortex formation, including arguments based on the role of the internal velocity of the drop at impact (see Chapman and Critchlow 1967), and the details of the crater formed by the impact (see Rodriguez and Mesler 1988; Peck and Sigurdson 1994, 1995). Once a drop-induced vortex ring is formed, it behaves in a manner identical to vortex rings formed by more traditional methods (e.g. by fluid suddenly ejected from an immersed orifice). Many studies of such vortices exist, and a review can be found in Shariff and Leonard (1992).

A particularly interesting characteristic of drop-induced vortices concerns the manner in which the penetration depth of the vortex varies with the height from which the originating drop was released. Plots of penetration depth versus drop height reveal periodic maxima and minima. This behavior has been observed by numerous researchers, including Thomson and Newall (1885), Chapman and Critchlow (1967), Rodriguez and Mesler (1988), Durst (1996), and Saylor and Grizzard (2003). These extrema have been attributed to the shape of the drop at the moment of impact with the water surface. This effect of drop shape on maximal vortex penetration is the subject of the present work.

Drop-induced vortices have been studied for well over a century, perhaps the first investigation being that due to Rogers (1858) who documented several methods for forming vortex rings, including the use of falling drops. The first detailed study of drop-induced vortex rings was conducted by Thomson and Newall (1885). These authors investigated a variety of liquids and drop sizes, and recorded many qualitative and quantitative aspects of these vortex rings. Among their quantitative observations was the fact that the vortices penetrated the liquid bulk particularly well for certain drop heights and quite poorly for other drop heights. They presented the first plot of penetration depth versus drop height, revealing the oscillatory nature of this plot.

Thomson and Newall (1885) attributed the periodic maxima and minima in their vortex penetration versus drop height plots to the oscillations of the falling drops. A falling drop will undergo shape oscillations having a frequency f defined as:

$$f = \frac{1}{\pi}\sqrt{\frac{2\sigma}{\rho R^3}} \tag{1}$$

where R is the radius of the falling drop, σ is surface tension and ρ is density (Rayleigh 1879). Nominally, these shape oscillations result in prolate and oblate shapes at the extremes of the cycle, achieving a spherical shape in-between.[1] For drops that are large and/or falling near terminal velocity, these shape oscillations are complicated; the drop shapes can deviate from a perfectly oblate or prolate shape and the oscillations can occur about an equilibrium shape that is non-spherical (Beard and Chuang 1987; Beard et al. 1989). However, for the small drops and small velocities which are considered in studies of drop-induced vortices, these deviations from the nominal oscillation pattern are expected to be small and are ignored herein. Therefore, we consider a falling drop that oscillates between a perfectly prolate and oblate shape and achieves a perfectly spherical shape in-between.

Thomson and Newall (1885) demonstrated that the separation in the peaks of their vortex penetration versus drop height plots could be related to the frequency of drop oscillation given in Eq. 1. Converting the spatial separation of the peaks to a temporal spacing using the acceleration of the drop caused by gravity, they found that this spacing compared very well to the natural oscillation period of the drop obtained from Eq. 1. Using this information they concluded that the degree of vortex penetration depends on the shape of the drop at impact.

Chapman and Critchlow (1967) performed a photographic study to further explore the findings of Thomson and Newall (1885) and to ascertain the exact shape of the drop at impact that causes maximal vortex penetration. They confirmed the results of Thomson and Newall (1885), finding peaks that were separated by a time spacing corresponding to the drop oscillation period.[2] They also found that the vortices that penetrated the deepest were obtained from drops that were spherical and in the phase of oscillation where the drop is transitioning from an oblate shape to a prolate shape. Conversely, when the drop was spherical and moving from a prolate to an oblate shape, vortex penetration was at a minimum. The authors suggested that the reason for these observations was related to the internal velocity field of the oscillating drop. A study very similar to that of Chapman and Critchlow (1967) was conducted by Durst (1996) who also found that maximum vortex penetration occurred for drops having a spherical shape at impact, and in the phase of oscillation where the drop was moving from an oblate to a prolate spheroid.

Rodriguez and Mesler (1988) investigated drop-induced vortices using high speed cinephotography and found, in contrast to the observations of Durst (1996) and Chapman and Critchlow (1967), that the most penetrating vortices were observed when the drop was prolate in shape and that the least penetrating vortices occurred when the drop was oblate. They provided an explanation for these observations based on the shape of the crater caused by drops of differing shape. The studies of Peck and Sigurdson (1994, 1995) also showed the importance of the impact crater during vortex formation. Finally, the work of Kutter (1916) also contradicts the results of Chapman and Critchlow (1967).

It is unclear what causes the differences in the observations of optimal drop shape in the aforementioned investigations. Most investigations of drop-induced vortices mention surface tension σ as an important parameter. Therefore, one might argue that the observed differences between investigators is due to varying levels of contaminating surfactants on the flat water surface, and a concomitant variation in σ. In the experiments due to Durst (1996), for example, great care was taken to control the temperature of the bulk so that the same surface tension existed throughout the experiments. Durst (1996) also notes that contamination of the free surface was a significant contributor to lack of repeatability. Neither Rodriguez and Mesler (1988) nor Chapman and Critchlow (1967) note any special precautions taken to prevent accumulation of contaminating surfactants on the flat water surface, although this does not mean that such precautions were not taken. Taken as a whole, these observations could be used to argue that variations in σ on the flat water surface due to varying surfactant contamination levels explain the resulting discrepancies regarding optimal drop shape for vortex penetration. An investigation due to Saylor and Grizzard (2003) explored this possibility. In this study, surfactants were purposely added to the flat water surface over a range of concentrations. The addition of surfactants was observed to have a significant effect on the amplitude of the peaks in the vortex velocity versus drop height plots (similar to the vortex penetration versus drop height plots discussed above). However the presence of surfactants on the flat water surface had no effect on the *location* of the peaks in these plots. Therefore, even significant variations in surfactant contamination on the flat water surface cannot explain the different drop shapes at which peak vortex penetration was observed by the aforementioned researchers.

An alternate possibility, which has not been investigated, concerns variations in the surface tension of the drop fluid. In the studies cited above, the surface tension of the drop fluid was used to compute the oscillation period using Eq. 1. However an unexplored possibility is that the presence of surfactants on the drop fluid and the concomitant change in surface tension of the drop surface might affect the *shape* at which optimal vortex penetration occurs. In the study presented here, a soluble surfactant, Triton X-100, is added to the drop fluid to determine if changes in the surface tension of the drop change the optimal shape at which vortices penetrate the water surface.

The work presented here finds application in the study of rain enhanced gas exchange. The impact of raindrops on a water surface is known to enhance the transport across the air/water interface of such dissolved gases as oxygen and carbon dioxide. This has been observed, for example, by Ho et al. (1997, 2000). This enhancement of gas exchange by rain can be significant in small bodies of water such as lakes and rivers, where enhancement by wave breaking and high wind speed (which dominates in

[1] In this paper, oblate refers to an ellipsoid with its major axis in the horizontal orientation, and prolate refers to an ellipsoid with its major axis in the vertical orientation.

[2] An exception was noted for low viscosity liquids such as Freon 11 and acetone, but only for the initial peak.

large bodies of water such as oceans) are absent. The mechanism by which this enhancement occurs is incompletely understood; however evidence exists suggesting that the vortices formed by drop impacts play an important role. For example, Durst (1996) observed that oxygen concentration profiles in lakes exhibited a maximum beneath the surface, a result that can be explained by vortex penetration and cannot be explained by turbulent or gradient driven transport alone. Hallet and Christensen (1984) demonstrated that the volume of fluid entrained by these laminar vortices can be as large as 100 times the volume of the vortex core, indicating that the enhancement of gas exchange by drop-induced vortices can be large.

A raindrop which strikes a water surface at terminal velocity does not itself typically form a vortex. However, the impact of a raindrop results in a splash that creates secondary drops, and these secondary drops can form vortices. For example, Lange et al. (2000) visualized the subsurface flow resulting from simulated raindrop impacts and observed the formation of vortices caused by the secondary drops. Because vortices formed by drop impacts incorporate the drop fluid into the vortex, such vortices can transport the atmospheric gases absorbed by the raindrops deeper into the fluid bulk by a distance that is significantly larger than would otherwise be the case. The results of the work presented here shed light on the physics of the vortex penetration process, thereby improving the understanding of rain enhanced gas exchange.

2 Experimental

The experimental method employed here is essentially identical to that described in Saylor and Grizzard (2003) where water drops free of surfactants were used exclusively. In the present work, the procedure was modified slightly to permit the use of water drops containing the surfactant Triton X-100. In the following description the method is recapitulated. Greater details regarding the experimental method can be found in Saylor and Grizzard (2003).

In the research cited in the previous section, the penetration characteristics of drop-induced vortices were quantified by the vortex penetration depth. In the present work penetration depth was found to be unsuitable. Background convective currents made it difficult to determine exactly when the vortex had stopped, causing the penetration depth measurement to be subjective. Instead of the penetration depth, the penetration velocity was recorded at a fixed location beneath the water surface. Therefore, plots of vortex velocity versus drop height are presented here, as opposed to penetration depth versus drop height as were presented in the literature cited above. Chapman and Critchlow (1967) present plots of vortex velocity versus vortex depth that are linear and whose slope does not change significantly with initial vortex velocity. This suggests that vortex velocity correlates well with the final vortex penetration depth.

The experimental apparatus is illustrated in Fig. 1. Drops were generated at the end of a 1.6 mm outer

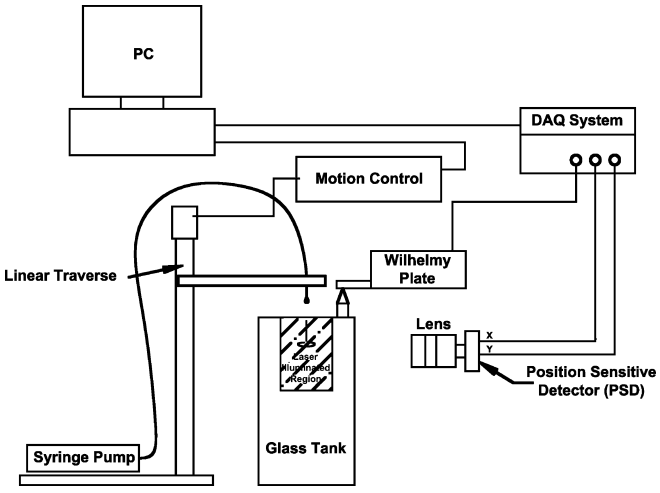

Fig. 1. Experimental apparatus

diameter Teflon tube which was supplied by a syringe pump. The tube was attached to a support arm, mounted on a vertical stage that was driven by a PC-controlled stepper motor. This system provided positioning of the droplet release point with a precision of ±0.02 mm. The drops fell into a glass tank which was filled to the rim. This tank was 40.0 cm in height and measured 16.0 cm×16.0 cm when viewed from above. The surface tension of the flat water surface was monitored using a Wilhelmy plate attached to a Sigma 703 tensiometer (KSV Instruments Ltd.).

Laser-induced fluorescence (LIF) was used to measure vortex velocity. The drop fluid contained a solution of disodium fluorescein in addition to the surfactant Triton X-100 (described further below). Therefore, the vortex formed by the falling drop contained a fluorescent dye. The measurement region was illuminated by an argon ion laser beam, causing the dyed vortex to fluoresce. This fluorescence was detected by a position sensitive detector (PSD) whose signal was used to measure the vortex velocity, as described below. The laser beam was expanded and collimated by a 12 mm/356 mm focal length lens combination separated by the sum of the focal lengths, as illustrated in Fig. 2. The bright portion of this expanded beam was approximately 8 cm in diameter and was

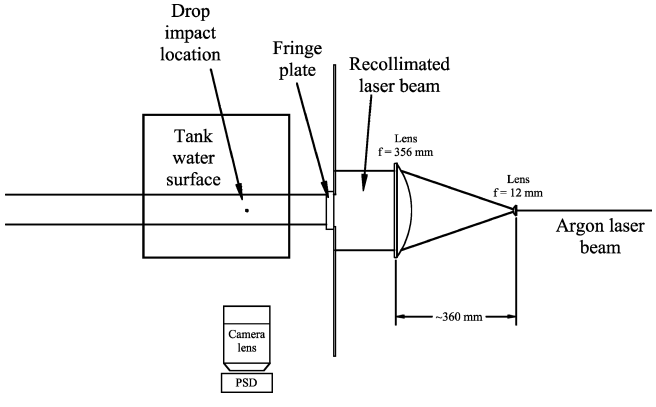

Fig. 2. Top view of apparatus

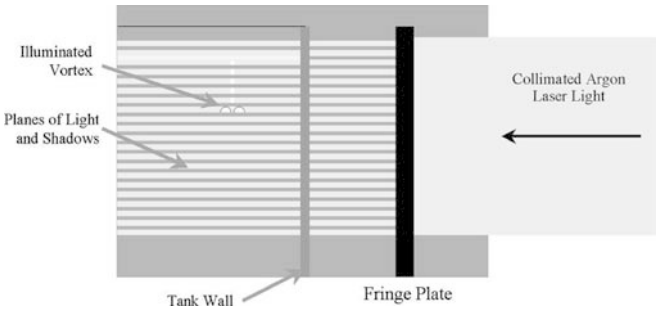

Fig. 3. Schematic of the measurement region (side view). Part of the collimated laser beam is blocked by the fringe plate, creating horizontal planes of light and shadow

directed at a fringe plate located on the outside of the tank. This plate blocked strips of the laser beam, creating horizontal slabs of light in the tank, each 1/16 inch thick and separated by 1/16 inch. A schematic of the "fringed" laser beam is presented in Fig. 3.

During operation, a vortex formed from a dyed drop penetrates into the illuminated region illustrated in Fig. 3. When observed from the side of the tank viewed by the PSD (Fig. 2), the vortex would periodically emit light as it passed through the fringed laser beam. A PSD detects the location of the centroid of the light which strikes its surface, providing an x and y output voltage that is linearly related to this centroid position. A 50 mm camera lens was placed in front of the PSD, facing the illuminated region of the tank where the vortices traveled. The PSD was shifted slightly off from the optical axis of the camera lens. When the vortex was absent or located within the dark fringes of the measurement region, the PSD output would give an approximately zero voltage.[3] When the vortex entered a laser fringe, the image of that vortex was focused onto a portion of the PSD displaced from the geometric center of the detector, resulting in an increase in both the x and y outputs. A sample time trace of one of the PSD outputs is presented in Fig. 4. The peaks in the signal correspond to the points in time where the vortex resided in the fringes of the laser beam. The separation in the peaks observed in this plot, Δt, and the known separation in the laser fringes, Δx, were used to compute the vortex velocity, v, via the equation:

$$v = \frac{\Delta x}{\Delta t} \tag{2}$$

A computer program was written to extract v from the PSD time traces. The largest peak observed in the time traces occurred at a location 14 mm beneath the water surface, which was the location where vortex velocity is reported here.

The outputs from the PSD and the Wilhelmy plate were acquired at 1000 Hz by a PC using a data acquisition card. Data acquisition and motion control of the drop release point were all controlled by a program written in the LabView environment.

[3]Actually a voltage corresponding to the centroid location of the laboratory background illumination.

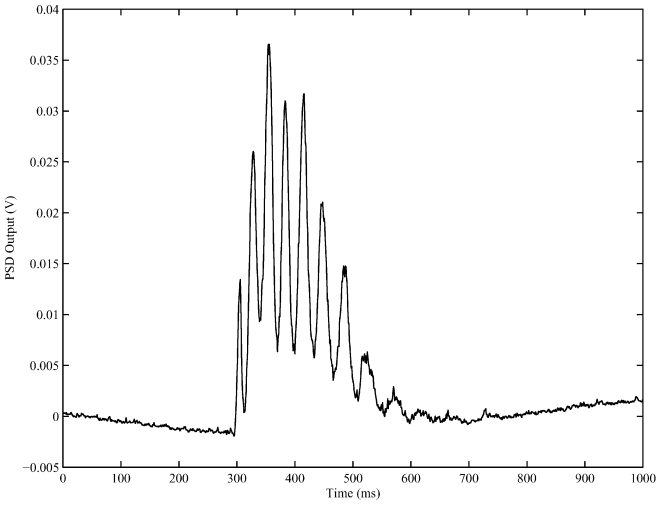

Fig. 4. Plot of PSD output voltage versus time, sampled at 1000 Hz. Motion of the vortex through the laser beam fringes causes the peaks in the signal. For this time trace, the drop fluid consisted of a 4 mg/L solution of Triton X-100, and the tank consisted of a 0.125 mg/L solution of Triton X-100. The drop was released from a height of 37 mm

In these experiments, all of the drops investigated consisted of a 4.0 mg/L solution of Triton X-100. The volume of these drops was 24.1 μL. An important variable in these experiments is the surface tension of the drops. Obtaining a surface tension measurement of the Triton X-100-containing drop surface was challenging since Triton X-100 is a soluble surfactant and the monolayer on a newly formed surface (such as that of a drop forming at a nozzle) is changing due to the growing surface area and diffusion of surfactant from the bulk of the pendant drop. As an estimate, the surface tension at the drop surface was assumed to change at a rate identical to that of a flat surface. Figure 5 shows surface tension time traces for 4.0 mg/L, 8.0 mg/L, and 16.0 mg/L Triton X-100 solutions in a tank. To obtain these time traces, the solutions were

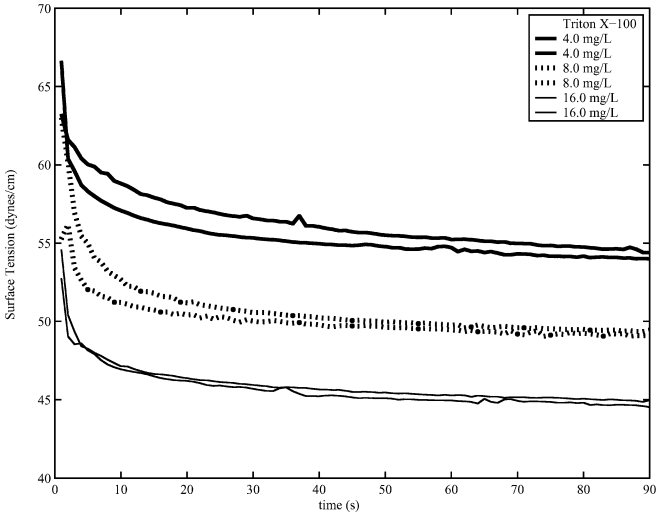

Fig. 5. Surface tension response following a swipe for solutions with different concentrations of Triton X-100. Two tests are performed with each solution to show reproducibility

prepared and the Wilhelmy plate was positioned just above the water surface. The surface was swiped (wiped across with a glass rod) and the Wilhelmy plate was then immediately attached to the surface. Surface tension was then recorded for 90 s. This procedure was followed twice for three concentrations. In these experiments, 4.0 mg/L Triton X-100 drops were used. These drops fell after forming on the nozzle for 25 s. Therefore, the surface tension of a 4.0 mg/L Triton X-100 solution was obtained from Fig. 5 by averaging the value of the two plots at this concentration at t=25 s, giving σ=56 dynes/cm.

Triton X-100 monolayers were also created on the surface of the tank. When forming these monolayers, the tank was first filled and the water surface cleaned by overflowing the tank and swiping the surface with a clean glass rod. Further details regarding the procedure used to insure cleanliness of the water can be found in Saylor and Grizzard (2003). The water level was then lowered by several centimeters and the Triton X-100 solution was added. Because surfactant can accumulate on the surface of bubbles, altering the bulk concentration, the Triton X-100 solution was added slowly to prevent splashing and bubble formation. Using a clean glass rod, the solution was stirred gently but thoroughly. Once the added Triton X-100 was dissolved, the tank was filled and then overfilled very slightly. The surface was then swiped to remove any contaminating (non-Triton X-100) surfactant accumulated during mixing. For experiments conducted without any surfactants (surfactant concentration of zero), doubly distilled water was added to the tank. The tank was overflowed and swiped with a glass rod, and experiments were then initiated.

Vortices were formed from drops falling from a height which ranged from 4.8–46.0 mm. Multiple vortices were recorded at each drop height. The drop fluid consisted of a 4.0 mg/L solution of Triton X-100 for all experiments. A range of Triton X-100 concentrations were explored on the flat water surface. The highest Triton X-100 concentration investigated was prepared first. The full drop height range was explored at this concentration, and the tank was then drained by 50% and filled again. This gave a new surfactant concentration which was half of the previous concentration. This procedure was continued until the concentrations c=4.0, 2.0, 1.0, 0.5, 0.25, and 0.125 mg/L were investigated. The zero concentration run was conducted last.

In the next section, the results obtained from these experiments are presented as plots of vortex velocity v versus drop height h. Drop height h is defined here to be the distance from the water surface to the nozzle.

3 Results

Figure 6 is a plot of v versus h for drops consisting of a 4.0 mg/L solution of Triton X-100. The concentration of Triton X-100 on the flat water surface varies from 0.0 to 4.0 mg/L, as indicated in the legend. The legend also indicates the surface tension of the flat water surface corresponding to each concentration. Figure 6 shows that the presence of surfactants on the flat water surface affects the penetration velocity. Specifically, vortex velocities at

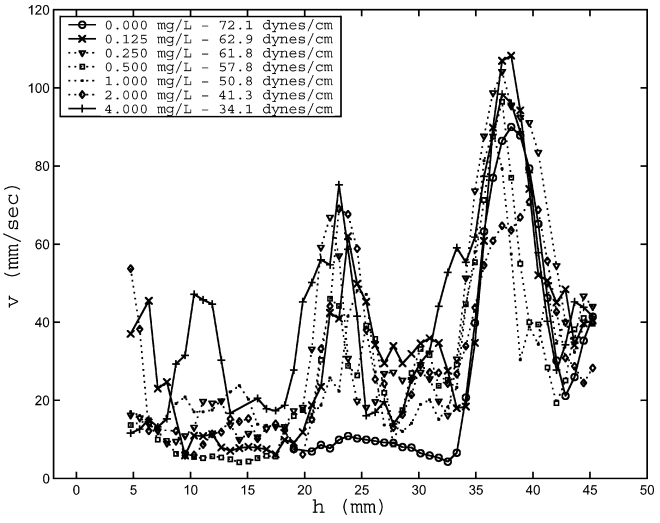

Fig. 6. Plot of vortex velocity versus drop height for water drops having a concentration of 4.0 mg/L of Triton X-100. The Triton X-100 concentration on the flat water surface is indicated in the legend

the peaks in these plots are not very large when the surfactant concentration is very large, or if it is zero. However, at intermediate surfactant concentrations the vortex velocity is maximized. The effect of the flat surface surfactant concentration on the vortex velocity is discussed in detail in Saylor and Grizzard (2003). Although the vortex velocities are significantly affected by variations in the surfactant concentration on the flat surface, the *locations* of the peaks are not affected at all by the flat surface surfactant concentration.

Figure 7 is a plot of v versus h, obtained from Saylor and Grizzard (2003), for experiments where the drop fluid was kept free of surfactants, in contrast to the present experiments. The flat surface concentrations considered in Fig. 7 are the same as in Fig. 6. The focus of the present work is on the shape of the falling drop which maximizes

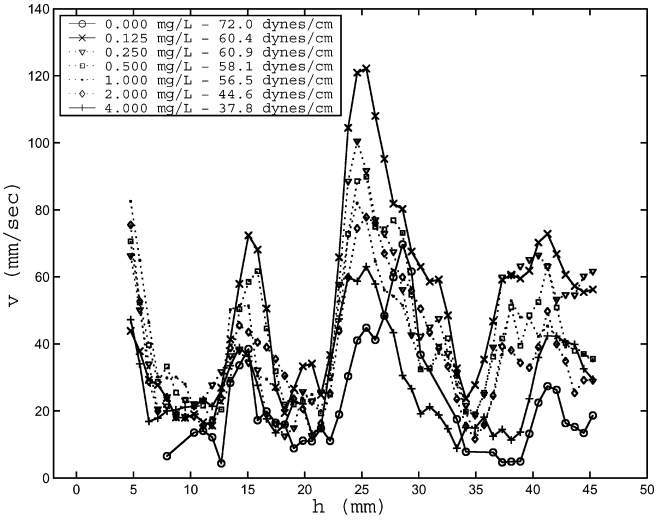

Fig. 7. Plot of vortex velocity versus drop height for water drops free of surfactant. The Triton X-100 concentration on the flat water surface is indicated in the legend

the vortex velocity. As described in Sect. 1, the shape of the drop at impact can be intuited from the location of the peaks in the v versus h curves. The peaks in Fig. 6 are at different values of drop height h, than in Fig. 7. Since the range of flat surface surfactant concentrations is identical in these two figures, it must be the presence of surfactant on the drop which accounts for the difference between these two sets of plots. To focus on the location of the peaks, the data presented in Figs. 6 and 7 are replotted together in Fig. 8 without the individual symbols that denote the flat surface concentration. This figure reveals that adding surfactant to the drop surface causes the peaks to shift to the left. The two largest peaks are identified as Peak 1 and Peak 2 in the figure. Both of these peaks are shifted to the left when comparing the surfactant-covered drops to the surfactant-free drops. The values of h for Peak 1 and Peak 2 for each of these two cases is presented in Table 1. The value of h presented is obtained by averaging the peak locations for each of the experiments presented in Fig. 7.

The literature on drop-induced vortices frequently employs the dimensionless Froude and Weber numbers to characterize the drop (see, for instance, Peck and Sigurdson 1994, 1995). These are defined as:

$$Fr = \frac{V^2}{2gR} \tag{3}$$

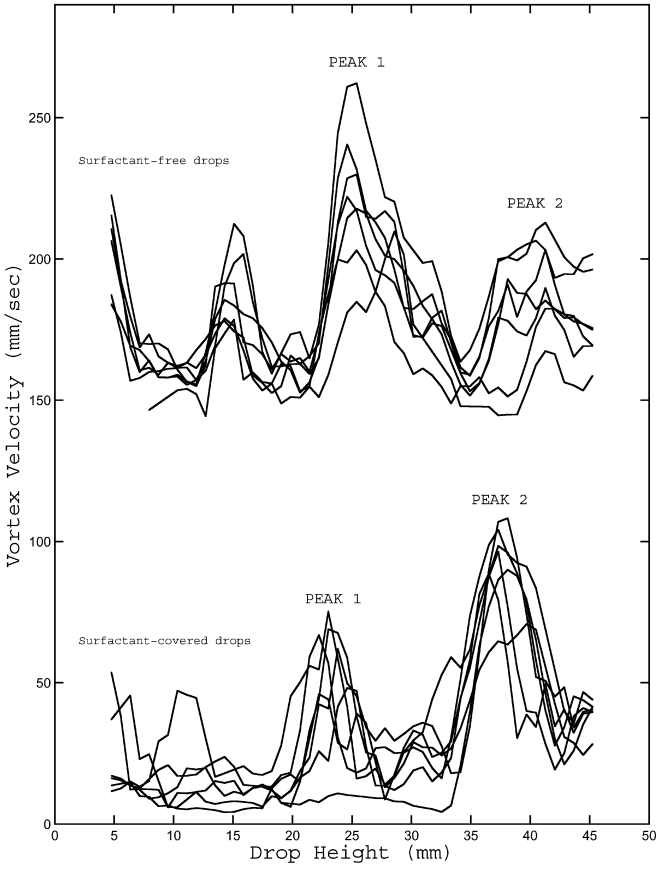

Fig. 8. Combination of Figs. 6 and 7 revealing the relative position of the peaks for experiments with surfactant-free and surfactant-covered drops. The two largest peaks are identified as Peak 1 and Peak 2 to aid comparison

Table 1. Values of h,V, Fr and $We$for Peaks 1 and 2 for surfactant-free drops and surfactant-covered drops

	h (mm)	Fr	We
Peak 1 surfactant-free	25.6	14.2	25.3
Peak 2 surfactant-free	40.8	22.3	39.8
Peak 1 surfactant-covered	23.1	12.8	28.7
Peak 2 surfactant-covered	37.9	21.1	47.3

and

$$We = \frac{2\rho V^2 R}{\sigma} \tag{4}$$

respectively, where V is the velocity of the drop at impact, R is the effective radius of the drop (the radius that a spherical drop having a volume equivalent to that of the oscillating drop would have), σ is the surface tension of the drop, g is the gravitational acceleration, and ρ is the density of the drop. To facilitate comparison with other work, values of Fr and We are presented in Table 1 for Peak 1 and Peak 2 for the surfactant-free and surfactant-covered cases. The values of ρ, R and σ used to obtain these numbers are presented in Table 2. The velocity at impact, V was not measured in these experiments, and so we calculate it from the fall height h, using the equation presented in Pumphrey and Elmore (1990):

$$V = V_{\mathrm{T}}\left[1 - \exp\left(\frac{-2gh}{V_{\mathrm{T}}^2}\right)\right]^{1/2} \tag{5}$$

where V_{T} is the terminal velocity which we obtained from the empirical relation due to Atlas et al. (1973) as presented in Doviak and Zrnić (1984):

$$V_{\mathrm{T}}(R) = 9.65 - 10.3\exp\left(-600R\right) \tag{6}$$

An explanation of the results presented in Fig. 7 is now presented.

4 Discussion

According to Eq. 1 defined in Sect. 1, surfactants affect f in two ways. First, they reduce surface tension, which reduces the numerator of Eq. 1. Second, as the surface tension is reduced, the volume at which the drop is released is also reduced, since the force attaching it to the nozzle is smaller. Therefore R is smaller, reducing the denominator. The drops used in the present study consisted of a 4 mg/L solution of Triton X-100 having a volume of 24.1 μL. The drops used in Saylor and Grizzard (2003) were free of surfactants and had a volume of 24.8 μL. This corresponds to a value of R=1.81 mm for the clean drops and R=1.79 mm for the surfactant-covered drops. To compute

Table 2. Predicted drop oscillation frequency for surfactant-free and Triton X-100 contaminated drops

	ρ (g/cm^3)	σ (dynes/cm)	R (cm)	f (Hz)
Surfactant-free drop	1.0	72.0	0.181	49.6
4.0 mg/L Triton X-100	1.0	56.0	0.179	44.5

f, R and σ are inserted into Eq. 1. The value of σ for the clean drop is 72 dynes/cm and for the surfactant-covered drop a value of 56 dynes/cm was used, as obtained from Fig. 5 as described in Sect. 2. The density of water is virtually unaffected by the Triton X-100 concentration used here and a value of ρ=1.0 g/cm^3 is used for both cases. The resulting values of f are presented in Table 2 for the surfactant-covered drops investigated here and the surfactant-free drops investigated in Saylor and Grizzard (2003). The reduction in R due to surfactant addition is small compared to the reduction in σ, and so there is a net decrease in the oscillation frequency f from 49.6 Hz to 44.5 Hz due to the presence of Triton X-100 in the drops used in the present experiments.

Because the drop shape at impact is determined by f, a difference in peak location for the clean and surfactant-covered drop cases should be expected. Stated another way, two drops released from the same height, but with different oscillation frequencies, will have different shapes upon impact. Therefore, some difference in the peak locations is expected for the data presented in Fig. 8. To determine if the difference in peak location can be explained solely by the difference in f, the data presented in Fig. 8 are replotted in Fig. 9 with superimposed plots showing the computed amplitude oscillation plots. These amplitude oscillation plots are simply the amplitude of drop oscillation as a function of fall distance for the given drop. Here we use the word "amplitude" loosely. It can be thought to be, for example, the ratio of the major axis to the minor axis of the drop. However the numerical amplitude does not correspond to a particular shape (prolate, oblate, or between), and its initial value is arbitrarily set to zero. The exact values of the amplitudes presented in this plot are not significant. What is significant for the present discussion is the location of the peaks in the amplitude oscillation plot relative to the peaks in the associated v versus h plot. If the difference in the two v versus h plots is due solely to differences in f, then the relative positions of the peaks in the drop amplitude oscillation plot and the v versus h plot should be the same regardless of whether surfactant is on the drop or not. This is not the case. For example, in the surfactant-free drop case, Peak 1 is located directly beneath Peak D in the corresponding drop amplitude oscillation plot. However for the surfactant-covered drop, Peak 1 is located half a drop oscillation ahead of Peak D. Similarly, Peak 2 is located directly beneath Peak E for surfactant-free drops, but half an oscillation ahead of Peak E for surfactant-covered drops.

What the above observations indicate is that for an equivalent drop shape at impact, the resulting vortex penetration behavior differs significantly, depending on the surface tension (or perhaps the elasticity) of the drop. Note that for each of the two amplitude oscillation plots presented in Fig. 9, the shape of the drop at each of the labeled peaks should be the same. For example, if the drop shape is prolate at Peak D for surfactant-free drops, it should also be prolate at Peak D for the surfactant-covered drops. Therefore, whatever shape the drop actually attains at Peak D, it results in maximal vortex penetration for surfactant-free drops (since the velocity is maximized at Peak D in this case), and minimal vortex penetration for the surfactant-covered drops. Stated another way, there is a 180° phase shift between these two cases.

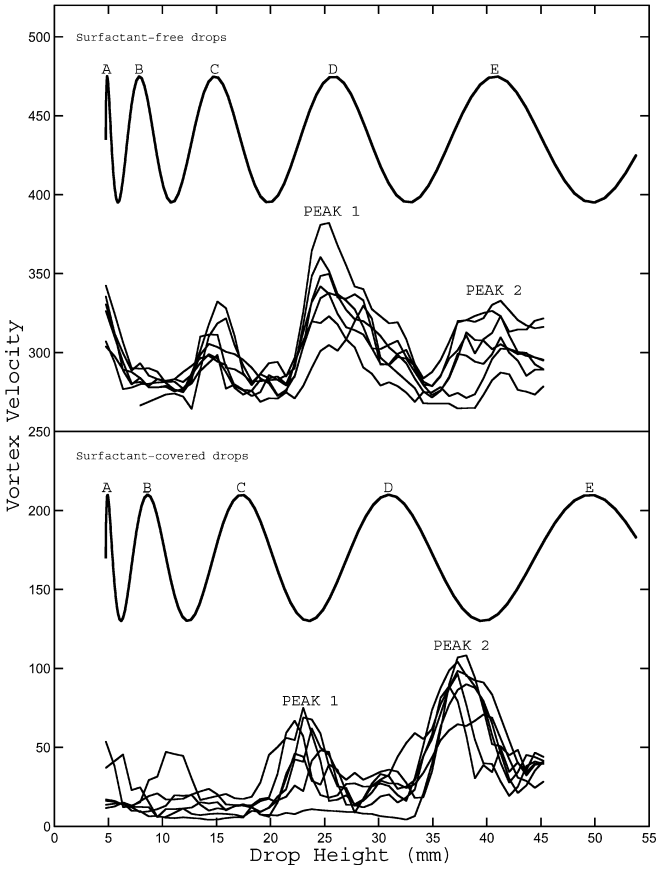

Fig. 9. Drop amplitude versus fall distance plots compared with v versus h plots. The upper pair of plots is for the case where the drop is free of surfactants. The lower pair of plots is for the case where the drop has a Triton X-100 monolayer. The upper plot in each pair containing alphabetically-labeled peaks is the plot of oscillation amplitude obtained using Eq. 1 using the known value of σ for the drop being considered (clean or surfactant-free)

These results are particularly interesting because they may explain contradictory observations reported in the literature. As was described in Sect. 1 Chapman and Critchlow (1967) observed that vortex penetration was maximized when drops impact with a spherical shape, changing from oblate to prolate. Rodriguez and Mesler (1988), on the other hand, observed penetration to be maximum when the drop is prolate at the moment of impact. These conclusions differ by a 90° shift in the phase of droplet oscillation. The present work suggests that both of the observations made by these authors may have been correct. These authors may have been investigating drops that, while nominally clean, actually had differing amounts of contaminating surfactants on the drop fluid. Water is notoriously difficult to maintain in a clean state (see Albrecht 1989; Saylor 2001), and neither authors reported on the precautions taken to minimize surfactant contamination in their drops.

It is noted that the above comparison relies on the assumption that the peaks labeled as '1' in the surfactant-free drop and surfactant-covered drop cases do

indeed correspond to each other. There is some reason for doubt regarding this assumption. Referring to the surfactant-covered drop data, one can see that the peak just prior to Peak 1 is really a peak for only one of the runs conducted. If this is not actually a peak, but simply spurious data, then the actual location of Peak 1 would correspond to the very first peak located at the beginning of the plot, and Peak 2 would be located in the position that is labeled Peak 1 in Fig. 9. We think the likelihood that this is the case is small. Nevertheless, even if it were so, the general conclusion obtained from the plots is the same: namely that the relative locations of the peaks in the data, compared to the location in the corresponding amplitude oscillation plots, are different for the surfactant-free and surfactant-covered cases. Indeed, no pairing of the data peaks to amplitude oscillation plot peaks can result in equivalent behavior for these two cases, indicating that the presence of the surfactant on the drop must change the shape at which optimal vortex penetration occurs.

Finally it is noted that, when compared to the amplitude oscillation plots, the data plots do not exhibit the closely spaced peaks referred to as "A" and "B" in the amplitude oscillation plots. Immediately after breaking off from the nozzle, the drop requires some period of time for oscillations due to the breakoff process to die out. This would almost certainly blur away the closely spaced peaks at the first few millimeters of drop fall. This is most likely the reason that these peaks are not actually observed in the data.

In the present work, drop shapes at the moment of impact were not directly observed, so the actual drop shape that causes greatest v for clean and contaminated drops cannot be postulated. What can be concluded from these data is that the presence of a surfactant on the drop does change the shape at which maximum penetration is achieved.

5 Conclusions

Measurements of the velocity of vortex penetration were made for vortices formed by falling water drops. These drops were covered with a monolayer of the surfactant Triton X-100. Comparison of vortex velocity versus drop height plots for these surfactant-covered drops with previously obtained plots for surfactant-free drops reveal differences in the peak locations in these plots. This difference in peak location cannot be solely attributed to the difference in drop oscillation frequency caused by the surface tension difference between surfactant-covered and surfactant-free drops. Rather, the primary cause of peak separation is due to a change in the drop shape at which optimal vortex penetration occurs for these two cases. Therefore, the presence of a surfactant monolayer on the falling drop affects the optimal shape for vortex penetration of drop-induced vortices.

References

Albrecht O (1989) Commonly used criteria for checking the cleanliness of Langmuir-Blodgett equipment and spreading solvents are not sufficient. Thin Solid Films 178:563–565

Atlas D, Srivastava RC, Sekhon R (1973) Doppler radar characteristics of precipitation at vertical incidence. Rev Geophys Space Phys 2:1–35

Beard KV, Chuang C (1987) A new model for the equilibrium shape of raindrops. J Atmos Sci 44:1509–1524

Beard KV, Ochs HT, Kubesh RJ (1989) Natural oscillations of small raindrops. Nature 342:408–410

Chapman DS, Critchlow PR (1967) Formation of vortex rings from falling drops. J Fluid Mech 29:177–185

Doviak RJ, Zrnić DS (1984) Doppler radar and weather observations. Academic, Orlando, FL

Durst F (1996) Penetration length and diameter development of vortex rings generated by impacting water drops. Exp Fluids 21:110–117

Hallet J, Christensen L (1984) Splash and penetration of drops in water. J Recherches Atmospheriques (Atmos Res) 18:225–242

Ho DT, Bliven LF, Wanninkhof R, Schlosser P (1997) The effect of rain on air-water gas exchange. Tellus 49:149–158

Ho DT, Asher WE, Bliven LF, Schlosser P, Gordan EL (2000) On mechanisms of rain-induced air-water gas exchange. J Geophys Res 105(24):45–57

Kutter V (1916) Die anwendung on wirbelringen zur bestimmung von oberflächenspannungen. Physik Z 23:573–579

Lange PA, van der Graaf G, Gade M (2000) Rain-induced subsurface turbulence measured using image processing methods. In: Proc 2000 Int Geoscience and Remote Sensing Symp (IGARSS 2000), vol. VII, Piscataway, NJ, 24–28 July 2000, IEEE, Washington, DC

Peck B, Sigurdson L (1994) The three-dimensional vortex structure of an impacting water drop. Phys Fluids 6:564–576

Peck B, Sigurdson L (1995) The vortex ring velocity resulting from an impacting water drop. Exp Fluids 18:351–357

Pumphrey HC, Elmore PA (1990) The entrainment of bubbles by drop impacts. J Fluid Mech 220:539–567

Rayleigh L (1879) On the capillary phenomena of jets. Proc R Soc Lond 29:71–97

Rodriguez F, Mesler R (1988) The penetration of drop-formed vortex rings into pools of liquid. J Colloid Interf Sci 121:121– 129

Rogers WB (1858) On the formation of rotating rings by air and liquids under certain conditions of discharge. Am J Sci 26:246–258

Saylor JR (2001) Determining liquid substrate cleanliness using infrared imaging. Rev Sci Instrum 72:4408–4414

Saylor JR, Grizzard NK (2003) The effect of surfactant monolayers on vortex rings formed from an impacting water drop. Phys Fluids 15:2852–2863

Shariff K, Leonard A (1992) Vortex rings. Annu Rev Fluid Mech 24:235–279

Thomson JJ, Newall HF (1885) On the formation of vortex rings by drops falling into liquids and some allied phenomena. Proc R Soc Lond 39:417–436